Journal of Petroleum Science and Technology 12(2): 42, 2025, Pages 38-49
DOI:10.22078/jpst.2025.5603.1966

Journal of Petroleum Science and Technology
Research Paper
https://jpst.ripi.ir/

# Syngas Production in a Sequential Fixed-bed Reactor Network Using Chemical Looping Reforming: A Numerical Analysis

**Sanaz Moradi Soltani[1], Hadi Ebrahimi [2] and Mohammad Rahmani[1]***
*1. Chemical Engineering Department, Amirkabir University of Technology, Tehran, Iran*
*2. Gas Research Division, Research Institute of Petroleum Industry (RIPI), Tehran, Iran*

## Abstract
Chemical looping reforming is a new technology for hydrogen or synthesis gas (syngas) production with lower $CO_2$ emission and energy usage than conventional routes such as methane steam reforming. In this study, the numerical analysis of syngas production in a packed-bed reactors' network is presented. Moreover, the proposed layout consists of four parallel reactors performing oxidation, reduction, and purge operations. In addition, both nickel and perovskite particles are used as the oxygen carrier. Furthermore, methane and oxygen were employed as fuel and oxidizer to produce $H_2$ and CO continuously. In addition, with the proper selection of temperature and reduction time, a dynamic study was carried out to evaluate the feasibility of the proposed system in terms of methane conversion (about 1), $H_2$ yield (about 0.65 mole $H_2$/mole $CH_4$), average syngas ratio (about 4 mole $H_2$/mole CO) and zero carbon dioxide at the reactor output. In the end, a switching system of the network is proposed for continuous syngas production..

***Keywords:*** Chemical Looping Reforming, Syngas Production, Continuous Process, Fixed bed Reactor, Oxygen Carrier.

## Introduction
Steam reforming is an established process for the production of both $H_2$ [1] and Synthesis gas (Syngas) [2]. Syngas is a mixture of hydrogen and carbon monoxide. The main industrial applications of the syngas are the production of liquid fuels over Fischer-Tropsch ($H_2$/CO=2), methanol ($H_2$/CO=2), ammonia($H_2$/CO=3), and alcohols synthesis [3]. Syngas could be converted into an H2-rich stream in which a further Water Gas Shift (WSG) stage is needed to convert the syngas into a mixture of $H_2$ and $CO_2$. For the sake of $H_2$ enrichment, a $CO_2$ separation unit, such as Pressure Swing Adsorption (PSA), is required [4].
More recently, Chemical Looping Reforming (CLR) in the fluidized bed reactors arose as a promising technology for hydrogen production [5]. CLR is a cyclic process in which a metal oxide serves as an oxygen carrier, usually Ni-based, which is alternatively oxidized exothermically by air in a fixed bed reactor. The heat generated in the air reactor can be used to drive endothermic steam reforming reactions in the Fuel reactor in such a way that the process is globally auto-thermic [5]. Therefore, direct contact between the fuel and air is avoided. As a result, an N2-free, $CO_2$-rich steam that can be easily purified in the view of $CO_2$ sequestration is obtained [6]. The main feature of this process is the synthesis of clean products, compared to the conventional steam reformer with a furnace. Among several sources of syngas, methane is the best fuel for hydrogen production due to its lowest pollution and large abundance all around the world [7] and relatively high H:C ratio [6].
A unified model for the gas-solid reactions for the NiO reduction by methane and the catalytic reactions was presented by Iliuta et al.[8].Moreover, two gas-solid reaction models of shrinking core model and volumetric particle were employed for the $NiO/Al_2O_3$ reduction by them [8]. The amount of $H_2$, CO, $CO_2$, $H_2O$, and unconverted CH4 were calculated by the model at the reactor outlet by the catalytic routes of both methane and $CO_2$ reforming. The model could also predict carbon formation inside the reactor. The model's results were proved using the experimental tests in a micro-fixed bed reactor. Diglio et al.[9] analyzed an autothermal CLR in the fixed bed to consider many challenges, namely the switching strategy between oxidation and reduction phases, the start-up temperature, and the cycle design, which must be addressed. They showed that hydrogen was produced in a very short period, below 30 s, in a Ni-based system. Ebrahimi and Rahmani [10] proposed a hydrogen production route in a chemical looping process in which the

**Corresponding author:* Mohammad Rahmani, Chemical Engineering Department, Amirkabir University of Technology, Tehran, Iran
*E-mail addresses:* m.rahmani@aut.ac.ir
*Received 2025-01-05, Received in revised form 10- 1-2025, Accepted 2025-01-06, Available online .....*

hydrogen was separated by a membrane layer after the production.

A novel approach was recently proposed by Spallina et al.[4], by using three reactors in which oxidation/reduction/reforming phases are sequentially operated. The employed model included a dedicated model for the radial heat losses from the reactor. They experimentally and numerically demonstrated that by carefully checking the heat management strategy, it was possible to reach a methane conversion of about 92%, a high H2 production, and inherent $CO_2$ capture.

A mathematical modeling of the syngas production was performed by Ebrahimi and Rahmani [3] by the perovskite oxygen carrier of La0.7Sr0.3-$FeO_3$ in the chemical looping process. Inside the reactor, some important parameters, such as reactant conversion, product compositions, and $H_2$/CO ratio, were analyzed.

A microreactor assembly was proposed by Ebrahimi and Rahmani [11] to thermally couple the reduction and oxidation reactors. The proposed geometry was mathematically modeled and analyzed. The configuration not only used the heat of oxidation but also mitigated temperature fluctuations inside the channels, which were harmful to all oxygen carriers. Effective parameters such as thermal conductivity, reaction rates, $H_2$ and CO production rates, and solid conversions were investigated.

A novel quasi-autothermal hydrogen production process was proposed by Diglio et al. [6]. The developed arrangement consisted of two sections: a CLC one that continuously produces a hot gas mixture of $H_2O$ and $CO_2$ at approximatively constant temperature and a reforming section devoted to hydrogen production employing two fixed beds driven by a gas stream leaving the CLC section. A methane conversion close to 100% and a very $H_2$-rich gas stream (average of 0.67) were evaluated. Almost all the $CO_2$ produced in the CLC section was converted in the reforming section, so overall $CO_2$ emissions were negligible, and a $CO_2$ separation unit was unnecessary.

In this study, a continuous process for syngas production is investigated. To the best of the authors' knowledge, no literature is available on modeling a complete cyclic process just using CLR, which shows that oxidation, reduction, and purging phases take place in a network of packed beds. Several works can be found in which each oxidation and reduction phase are separately modeled and optimized, or the process has been coupled with a fixed bed chemical looping combustion (CLC) with both steam and dry methane reforming. Moreover, sensitivity analysis was performed to determine suitable reactors and time sequence conditions. In this paper, the effect of key parameters on NiO, such as initial temperature, inlet temperature, comparison of NiO and perovskite oxygen carrier, residence time in the reduction reactor, and coke formation, are studied. Moreover, the product distribution, methane conversion, $H_2$ yield, and syngas ratio are shown inside the reactor.

This article is structured as follows. Section Mathematical Model presents the proposed system configuration, reactors, reactions scheme, and a packed-bed chemical looping reforming model. The model is validated by the results available in the literature [8]. In Section Results and Discussion, the main numerical results are reported. Firstly, the operation of a single-packed bed working under CLR conditions is discussed. Based on these results, a possible approach to operating several CLR reactors in parallel to obtain the continuous production of a gas mixture of $H_2$ and CO is assessed.

## Materials and Methods

### Mathematical Model

The conceptual scheme of the proposed system is reported in Fig. 1. The stationary CLR is a cyclical process packed with catalyst (particles), which is alternately exposed to oxidizing and reducing conditions via periodic switching of the gas feed streams, keeping the flow direction constant in both phases. During a time length toxi (oxidation time) the fixed bed reactor is fed by air where the oxidation of the oxygen carrier takes place; the fed composition is then changed to methane and, over a time length tred (reduction time) where the steam methane reforming and oxygen carrier reduction occurs. These two distinct steps are oxidation (OP) and reduction phases (RP). Due to very high O2–H2 reactivity, the formation of potentially explosive gas mixtures during gas switching between OP and RP and vice versa should be carefully avoided: during practical operations, this task is accomplished by feeding for a few instants an inert (purge phase) at the end of each OP and RP.

The simple idea behind the proposed scheme is that, by operating several reactors in parallel under the CLR conditions, continuous production of a mixture of $H_2$ and CO can be achieved.

To model the system mass transfer of gas species, solid conversion and both gas-solid and catalytic reactions inside the reactor are considered. More details about the model are presented below.

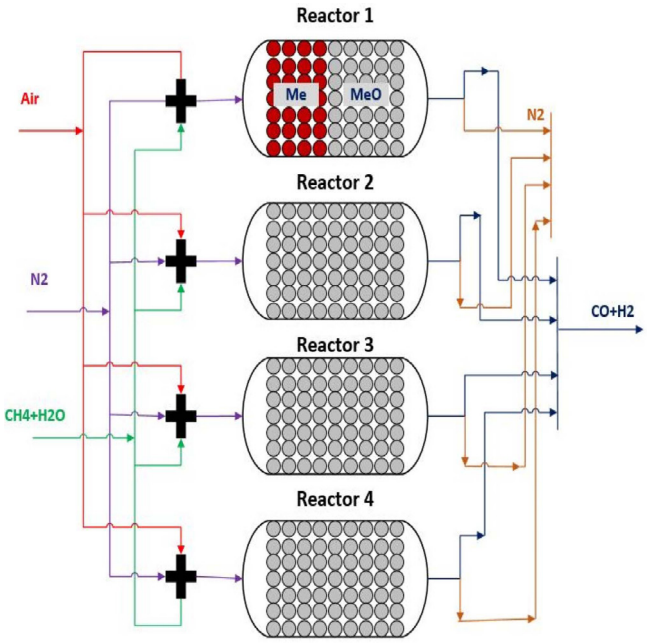


**Fig. 1** Conceptual scheme of the proposed system.

### Geometry and Reactor Conditions

The geometry of the fixed-bed reactor was selected from the previous work [9] performed for the investigation of the dynamic kinetics of NiO oxygen carriers under isothermal conditions. During the cyclic process, $N_2$ gas was used as an inert for the purging between both the reduction and oxidation. A three-point valve was used for switching the feeds.

Geometry and operating conditions of the reactors and oxygen carrier characteristics are reported in Table 1.

**Table 1** Reactor specifications used for the modeling.

| Parameter | Value |
|---|---|
| Reactor dimensions | |
| Reactor length (m) | 0.223 |
| Reactor diameter (cm) | 6 |
| Oxygen carrier | |
| Material | Ni (15%) Al2O3 |
| Particle diameter (μm) | 140 |
| Specific surface area($m^2/g$) | 102 |
| Bulk density ($kg/m^3$) | 1040 |
| Bed porosity | 0.37 |
| Operating conditions | |
| The inlet flow rate of the feed ($m^3/s$) | 1.98e-4 |
| Inlet Temperature (K) | 723 |
| Initial Temperature (K) | 1073 |
| Pressure (bar) | 1 |

### Internal and External Resistance

Internal and external diffusions are considered before applying rate-limited kinetics. External diffusion of the reactant to the surface is evaluated by the comparison of the radial mass flux of methane calculated by Frossling's correlation of:

$$W_{CH_4,r} = \frac{2D_{CH_4-N_2}}{d_p}(C_{CH_4,b} - C_{CH_4,s}) \quad (1)$$

and the observed reduction rate for the spherical particles of NiO:

$$-r_{CH_4,obs} = \frac{N_{CH_4,0}}{W a_0}\frac{dX}{dt} \quad (2)$$

Representation of all parameters is found in the reference [12].

Table 2 presents the employed parameters to evaluate both external and internal diffusion limitations. According to this table, the radial mole flux of methane is much higher than the observed reaction rate or $W_{CH4;r} >> r_{CH4;obs}$. Therefore, the external diffusion could be ignored. For internal diffusion limitation, the Weisze-Prater equation is applied [13]:

$$C_{WP} = \frac{-r_{CH_4,obs}\rho d_p}{D_{eff}C_{CH_4,b}} \quad (3)$$

The results (see Table 2) shows that CWP is much smaller than one, which means there is no mass diffusion inside the solid particles

**Table 2** Parameters used to evaluate external and internal diffusions.

| Parameter | Value (for internal diffusion) | Value (for external diffusion) |
|---|---|---|
| $D_p$ (mm) | 0. 14 | 0. 14 |
| $D_{AB}$ ($m^2/s$) | 0.361e-4 | 0.361e-4 |
| $C_{CH4,b}$ ($mol/m^3$) | 10.95 | 10.95 |
| $C_{CH_4,S}$ ($mol/m^3$) | - | 0 |
| W(g) | 1 | 1 |
| $W_{CH_4;r}$ ($mol/m^2s$) | - | 5.6 |
| $-r_{CH_4,obs}$($mol/m^2s$) | 2e-6 | 2e-6 |
| CWP | 0.0007 | 0.0007 |

According to the results of previous studies carried out by Han et al. in 2013 [14] and Iliuta et al. [8], heat and mass gradients inside and outside the oxygen carriers with a diameter below 200 , can be neglected. Therefore, the below assumption on internal resistance is valid.

### Assumptions

The following assumptions were applied to the model:

- A 1D model was assumed in the fixed bed reactor.
- Because of low pressure and high temperature, an ideal gas law was employed.
- Time-dependent study was considered to analyze the reduction of oxygen carrier while the syngas is produced.
- The reactor is adiabatic.
- Both convection and dispersion terms are considered for the mass and energy equation.
- The thermal resistance between the gas and solid phases is ignored, so the gas and oxygen carriers are in temperature equilibrium. (The calculated difference between the solid phase and the gas phase is less than ≈10 ◦C (Froment and Bischoff, 1979; Levenspiel, 2002), which points to a negligible resistance for external heat transfer.)
- The effects of internal penetration and external mass transfer are ignored.

### Reaction Kinetics Network

The mathematical model developed takes into account the reduction reaction mechanisms proposed by Iliuta et al. [8] to describe the reactions between methane and Ni-oxygen carrier. Furthermore, the oxidation of the Ni oxygen carrier is modeled using the work of Dueso et al. [15]. Table 3 summarizes reactive schemes and associated enthalpy variations used in the present work.

Non-catalytic reduction reactions of the oxidation of $CH_4$ ($R_{S1}$ and $R_{S4}$), $H_2$ ($R_{S2}$) and CO ($R_{S3}$), followed by catalytic reduction reactions, namely steam ($R_1$) and dry ($R_2$) reforming, water gas shift ($R_5$), methane decomposition ($R_3$), and carbon gasification both by water $R_7$) and by carbon dioxide ($R_6$) were accounted in the model.

The rates of the oxidation reactions ($R_8$) [15] and of the non-catalytic gas-solid reductions ($R_{S1}$-$R_{S4}$) have been expressed according to the volumetric particle model theory [8] and their analytical expressions are reported in Tables 4 and 5. reports the expressions of catalytic reaction rates ($R_1$-$R_7$) [8].

**Table 3** Reactive scheme and associated standard enthalpy of reactions.

| Noncatalytic reduction reactions | $\Delta H_{1200}$ (kJ/mol) | Reaction |
|---|---|---|
| $CH_4 + 2NiO \rightarrow 2Ni + 2H_2 + CO_2$ | 162 | $R_{s1}$ |
| $H_2 + NiO \rightarrow H_2O + Ni$ | -16 | $R_{s2}$ |
| $CO + NiO \rightarrow CO_2 + Ni$ | -49 | $R_{s3}$ |
| $CH_4 + NiO \rightarrow Ni + 2H_2 + CO$ | 211 | $R_{s4}$ |
| **catalytic reduction reactions** | | |
| $CH_4 + H_2O \rightarrow 3H_2 + CO$ | 227 | $R_1$ |
| $CH_4 + CO_2 \rightarrow 2H_2 + 2CO$ | 259 | $R_2$ |
| $CH_4 + Ni \rightarrow Ni\text{-}C + 2H_2$ | 91 | $R_3$ |
| $3H_2 + CO \rightarrow -CH_4 + H_2O$ | -227 | $R_4$ |
| $CO + H_2O \rightarrow CO_2 + H_2$ | -33 | $R_5$ |
| $C + CO_2 \rightarrow 2CO$ | 169 | $R_6$ |
| $C + H_2O \rightarrow CO + H_2$ | 136 | $R_7$ |
| **Oxidation reaction** | | |
| $O_2 + 2Ni \rightarrow 2NiO$ | -468 | $R_8$ |

**Table 5** Catalytic gas–solid kinetics.

$$r_{R_1} = \frac{\frac{k_{R_1} C_{CH_4} C_{H_2O}^{0.5} (R_m T)^{0.25} [1 - \frac{C_{CO} C_{H_2}^3 (R_m T)^2}{K_{P,R1} C_{CH_4} C_{H_2O}}}{C_{H_2}^{1.25}}}{(1 + K_{CO,R_1} C_{CO} R_m T + K_{H_2,R_6} C_{H_2}^{0.5} (R_m T)^{0.5} K_{H_2O,R_6} \frac{C_{H_2O}}{C_{H_2}})^2} \quad (6)$$

$$r_{R_2} = \frac{k_{R_7} C_{CH_4} C_{CO_2} (R_m T)^2}{1 + K_{CO_2,R_7} C_{CO_2} R_m T} \quad (7)$$

$$r_{R_3} = \frac{k_{R_3} K_{CH_4,R_3} (C_{CH_4} R_m T - \frac{C_{H_2}^2 (R_m T)^2}{K_{P,R_3}})}{(1 + \frac{C_{H_2}^{1.5} (R_m T)^{1.5}}{K_{H_2,R_3}} + K_{CH_4,R_3} C_{CH_4} R_m T)^2} \quad (8)$$

$$r_{R_4} = \frac{k_{R_4} K_{CO,R_4} K^2_{H_2,R_4} (C_{CO} R_m T)^{0.5} (C_{H_2} R_m T)}{(1 + K_{CO,R_4} (C_{CO} R_m T)^{0.5} + K_{H_2,R_4} (C_{H_2} R_m T)^{0.5})^3} \quad (9)$$

$$r_{R_5} = \frac{\frac{k_{R_5} C_{CO} C_{H_2O}^{0.5} R_m T}{C_{H_2}^{0.5}} [1 - \frac{C_{CO} C_{H_2}}{K_{P,R_8} C_{CO} C_{H_2O}}]}{(1 + K_{CO,R_1} C_{CO} R_m T + K_{H_2,R_1} C_{H_2}^{0.5} (R_m T)^{0.5} + K_{H_2O,R_1} \frac{C_{H_2O}}{C_{H_2}})^2} \quad (10)$$

$$r_{R_6} = \frac{\frac{k_{R_6}}{K_{CO_2,R_6} K_{CO,R_6}} [\frac{C_{CO_2}}{C_{CO}} - \frac{C_{CO_2} R_m T}{K_{P,R_6}}]}{(1 + K_{CO,R_6} C_{CO} R_m T + \frac{1}{K_{CO_2,R_6} K_{CO,R_6}} \frac{C_{CO_2}}{C_{CO}})^2} \quad (11)$$

$$r_{R_7} = \frac{\frac{k_{R_7}}{K_{H_2O,R_7}} [\frac{C_{H_2O}}{C_{H_2}} - \frac{C_{CO} R_m T}{K_{P,R_7}}]}{(1 + K_{CH_4,R_7} C_{CH_4} R_m T + \frac{1}{K_{H_2O,R_7}} \frac{C_{H_2O}}{C_{H_2}} + \frac{1}{K_{H_2,R_7}} C_{H_2}^{1.5} (R_m T)^{1.5})^2} \quad (12)$$

**Table 4** Non-catalytic gas-solid kinetics and their parameters ($k_{si}=k_{si,0}$ exp $(-E_{a,si}/RT)$).

| Reaction | $E_{a,si}$ (Jmol$^{-1}$) | $k_{si,0}$ (m/s) |
|---|---|---|
| $r_{R8} = a_0 X k_{s1} C(O_2) C_{Ni}^{0.7}$ | 22000 | 8.4e-3 |
| $r\_R_{s1} = a_0 (1\text{-}X) k_{s2} C_{CH_4} C_{Ni} C_{NiO}$ | 77416 | 4.66 |
| $r R_{s2} = a_0 (1\text{-}X) k_{s3} CH_2 C_{NiO}$ | 26413 | 1.31e-4 |
| $r R_{s3} = a_0 (1\text{-}X) k_{s4} C_{CO} C_{NiO}$ | 26505 | 1.097e-4 |
| $r R_{s4} = a_0 (1\text{-}X) k_{s5} C_{CH4} C_{Ni} C_{NiO}$ | 23666 | 4.18e-3 |

The rate of consumption or formation of i-species (i = X, NiO, Ni, $CH_4$, $H_2$, $H_2O$, CO, $CO_2$, $O_2$, $N_2$, C), ri, is determined by summing up the reaction rates of that species in all the reactions Rj(j = 1, 2, . . ., see Table 3). Therefore, the reaction rate of each species can be expressed as:

$$r_x = 2r_{R_{s1}} + r_{R_{s2}} + r_{R_{s3}} + r_{R_{s4}} - 2r_{R_8} \quad (13)$$

$$r_{NiO} = -r_x M_{NiO} \quad (14)$$

$$r_{Ni} = r_x M_{Ni} \quad (15)$$

$$r_{CH_4} = -(r_{Rs1} + r_{Rs4} + (r_{R1} + r_{R2} + r_{R3}) C_{Ni}) \quad (16)$$

$$r_{H_2} = 2r_{R_{s1}} - r_{R_{s2}} + 2r_{R_{s4}} + (3r_{R_1} + 2r_{R_2} + r_{R_5} + 2r_{R_3} + r_{R_7}) C_{Ni} \quad (17)$$

$$r_{H_2O} = r_{R_{s2}} - (r_{R_1} + r_{R5} + r_{R7}) C_{Ni} \quad (18)$$

$$r_{CO_2} = r_{R_{s1}} + r_{R_{s3}} - (r_{R_2} + r_{R_6} - r_{R_5}) C_{Ni} \quad (19)$$

$$r_{CO} = -r_{R_{s3}} + r_{R_{s4}} + (r_{R_1} + 2r_{R_2} - r_{R_5} + 2r_{R_6} + r_{R_7}) C_{Ni} \quad (20)$$

$$r_C = (r_{R_3} - r_{R_6} - r_{R_7}) C_{Ni} \quad (21)$$

$$r_{O_2} = -r_{R_8} \quad (22)$$

$$r_{N_2} = 0 \quad (23)$$

**Governing Equations**

To describe the axial temperature and concentration profiles in the packed-bed CLR reactor, a numerical 1D packed bed reactor model has been used. In Table 6 the model equations for both oxidation phase (OP) and reduction phase (RP) and the corresponding boundary conditions are reported. The mathematical model needs to be completed with appropriate initial conditions. To avoid the formation of potentially explosive gas mixtures ($O_2$–$H_2$) when the fed is switched by OP to RP and vice-versa, a purge phase is fed for few instants between the oxidation/reduction phases. The purge phase affects neither the concentrations of chemical species nor, due to the high catalyst heat capacity, the reactor temperature. For the evaluation of temperature dependences of gas properties and transport coefficients, state-of-the-art correlations and assumptions were adopted from Han et al.[14] and references therein.

## Results and Discussion

### Solution Procedure and the Model Validation

The numerical model has been solved using the commercial software package Python.

**Table 6** The mathematical model for the oxidation and reduction phases with corresponding boundary conditions.

| | |
|---|---|
| **Oxidation phase** | |
| Mass balance in the gas phase | $\frac{\partial C_i}{\partial t}=\frac{(\varepsilon_g \frac{\partial(D_{ax,i}\frac{\partial C_i}{\partial z})}{\partial x}-u_g\frac{\partial C_i}{\partial z}-r_i\rho_{OC})}{\varepsilon_g}$ (24) |
| Mass balance in the solid phase | $\frac{dC_{Ni}}{dt}=-2r_{R_1}M_{Ni}$<br>$\frac{dC_{NiO}}{dt}=-2r_{R_1}M_{NiO}$<br>$\frac{dX}{dt}=\frac{-2r_1}{C^0_{Ni}}$ (25) |
| Enthalpy balance | $\varepsilon_g\frac{\partial(\lambda_{eff}\frac{\partial T}{\partial z})}{\partial z}-u_gC_{p,g}C_{T,g}\frac{\partial T}{\partial z}-$<br>$\Delta H_{R_1}r_{R_1}\rho_{OC}=C_{p,g}C_{T,g}\frac{\partial T}{\partial t}$ (26) |
| **Reduction phase** | |
| Mass balance in the gas phase | $\frac{\partial C_i}{\partial t}=\frac{(\varepsilon_g \frac{\partial(D_{ax,i}\frac{\partial C_i}{\partial z})}{\partial x}-u_g\frac{\partial C_i}{\partial z}-r_i\rho_{OC})}{\varepsilon_g}$ (27) |
| Mass balance in the solid phase | $\frac{dC_c}{dt}=r_c$<br>$\frac{dC_{Ni}}{dt}=r_xM_{Ni}$<br>$\frac{dC_{NiO}}{dt}=-r_xM_{NiO}$<br>$\frac{dX}{dt}=\frac{2r_x}{C^0_{NiO}}$ (28) |
| Enthalpy balance | $\varepsilon_g\frac{\partial(\lambda_{eff}\frac{\partial T}{\partial z})}{\partial z}-u_gC_{p,g}C_{T,g}\frac{\partial T}{\partial z}+$<br>$\sum_{j=2}^{j=11}(-\Delta H_j)r_{R_j}\rho_{OC}=C_{p,g}C_{T,g}\frac{\partial T}{\partial t}$ (29) |
| Boundary condition | $\frac{\partial C_i(0,t)}{\partial z}=\frac{u_g}{\varepsilon_gD_{ax,i}}(C_i(0,t)-C_{i,IN})$<br>$\frac{\partial C_i(L,t)}{\partial z}=0$<br>$\frac{\partial T(0,t)}{\partial z}=\frac{u_gC_{p,g}C_{T,g}}{\varepsilon_g\lambda_{ax}}(T(0,t)-T_{IN})$ (30)<br>$\frac{\partial T(L,t)}{\partial z}=0$ |

The model includes a set of partial differential equations (PDE) that are obtained from mass and energy balance and a number of nonlinear algebraic equations and auxiliary relations. The partial differential equations are converted into a set of ordinary differential equations using the method of line (MOL) and then discretization is done along the length of the reactor by the finite difference method. The Implicit backward differentiation formula (BDF) was used for time stepping of the solver. To validate the modeling strategy, at first the model based on the work presented by Iliuta et al. [8] was implemented and compared against experimental data. Fig. 2 reports molar fractions of gas products at the exit of the packed-bed reactor. Noteworthy, the model is able to qualitative describe the time trend of experimental values. Iliuta et al. [8] concluded that the experimental outlet gas concentration signal was delayed because of the residence time of the gases between the valve and the gas analyzer. In this section, the numerical results of a single reduction step are reported. Subsequently, the variation of parameters such as reduction time, initial temperature, inlet temperature for the process was taken into account and the effects on the feasibility of CLR process were addressed. Finally, the results for the cyclic process after several alternating cycles and continuous process are presented and discussed.

## Reduction Phase

Fig. 3 shows the outlet gas molar fraction versus time. At first, due to the non-catalytic reactions, the amount of $H_2O$ and $CO_2$ increases suddenly. Shortly afterwards, the amount of water increases slowly due to the reaction $R_3$ to reach its maximum value of 0.72, while the concentration of carbon dioxide decreases from 0.28 to zero. After 50 seconds, the catalyst is completely reduced.

After that, $H_2$ and CO gases increase and water vapor decreases as a result of $R_6$-$R_{11}$ reactions. The methane conversion rate reaches its maximum value after 65 seconds, leaving the reactor unreacted due to the completion of gas-solid reactions by surface and network oxygen. The value of CO and $H_2$ reaches their highest value, 0.18 and 0.67, respectively, after 75 seconds. After this time, due to the reduction of heat in the reactor, the concentration of methane increases, and the concentration of hydrogen and carbon monoxide decreases. Fig. 4 shows the $CH_4$, $H_2$, and CO concentrations during the reactor reduction. According to methane distribution (a), methane is seen at 60 s at the outlet of the reactor. After that, methane is converted more, particularly at the outlet when the reactant is distributed along the reactor. In addition, methane is reduced from about 7 mol/m$^3$ to 2.5 mol/m$^3$ after 84 s at the end of the reactor. It is increased after that due to a gradual decrease in the reaction rates. Both $H_2$ and CO (b, c) are more produced at the end of the reactor when the products leave it. After 72 s due to the decrease in the reaction rates, these products decrease at the output of the reactor.

## Reaction Rates

At the beginning of the reduction cycle, non-catalytic reactions $r_1$, $r_2$, $r_3$ and $r_4$ dominate the catalytic reactions due to the presence of excess nickel oxide. Fig .5 shows the reaction rates at 5, 25, 65, and 85 seconds. As can be seen, after 25 seconds, the rate of non-catalytic reactions decreased, and the rate of reactions $r_1$, $r_2$, $r_3$ and $r_4$ and $r_5$ are increased.

## Carbon Deposition

One critical aspect of methane catalytic reforming is the formation of solid carbon on the surface of the catalyst, which may be caused by cracking reactions of methane or reverse reactions of carbon gasification with carbon monoxide and water vapor. Because methane is the only source of carbon production, carbon appears mostly in the reactor inlet.

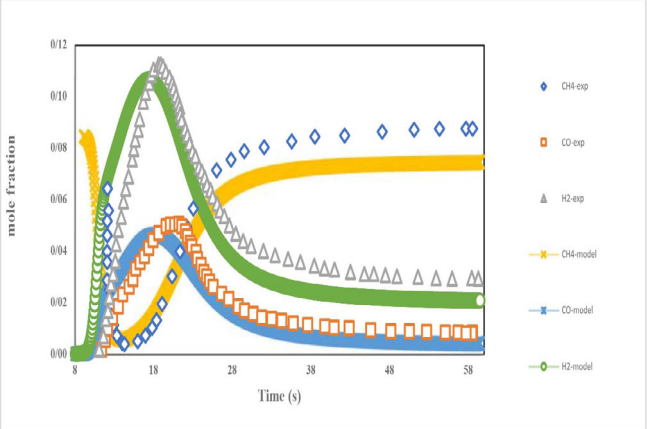


**Fig. 2** Experimental (dots, Iliuta et al. [8] and modeling (lines) outlet gas molar fraction.

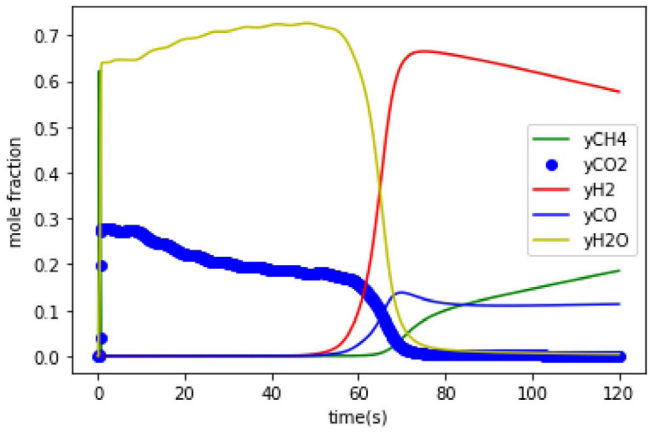


**Fig. 3** Outlet gas molar fraction versus time.

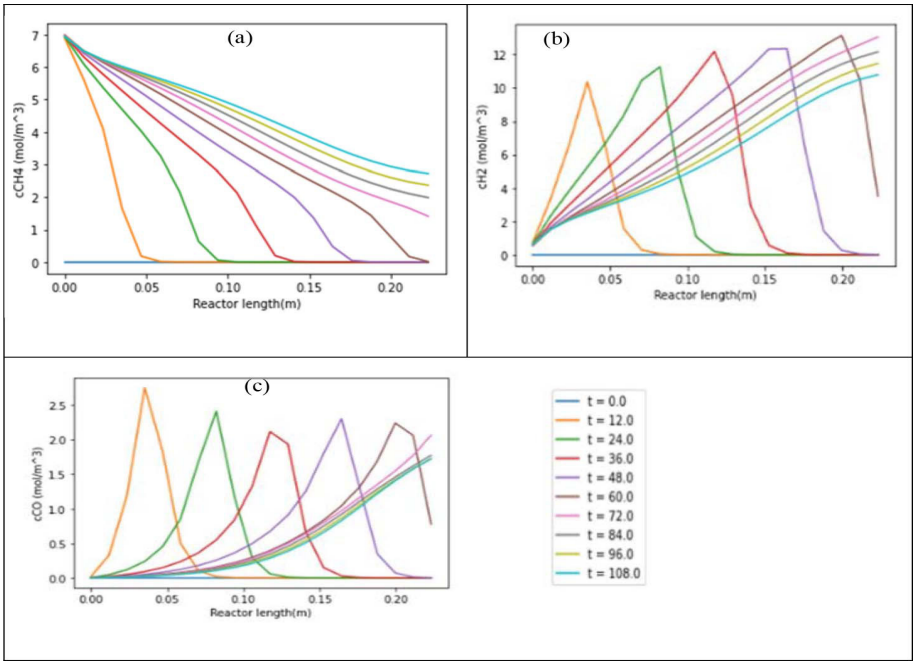


**Fig. 4** Methane, Hydrogen, and carbon monoxide concentrations inside the reactor at different times.

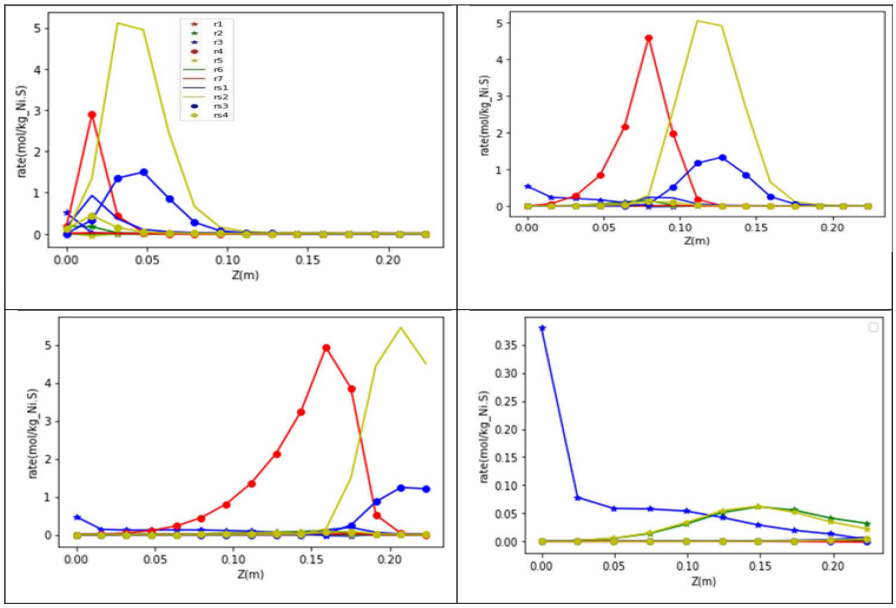


**Fig. 5** Reduction rate profiles at the fixed times (5, 25, 65, 85 s) during the reduction cycle.

In fact, after several times when nickel oxide is reduced during gas-solid reactions, unreacted methane reacts with the nickel created in this area and leads to the formation of carbon and the deactivation of the catalyst. In Fig.6, a carbon deposit actually builds up, which is equal to 0.07 kg-C/kg-OC, i.e., about 7 wt.%, a value close to that reported by Chiron et al. [16] as the upper limit before catalyst deactivation occurs in microreactor (about 5 wt%). Moreover, it is important to underline here that the kinetic scheme adopted in the present work does not account for carbon oxidation that eventually occurs during the OP. In addition, this reaction would have further reduced the amount of deposited carbon.

**Effect of the Initial and Inlet Temperature**

Fig.7 (a) shows that increasing the temperature causes an increase in the solid conversion at a lower time. The solid particles are converted faster at higher initial temperatures. Fig.7 (b) indicates that increasing the initial temperature causes an increase in the $H_2$ production. In Fig.7 (c, d), this rule is established for the syngas ratio and deposited carbon. However, the effect of inlet temperature in Fig.8 is inverse for these parameters.

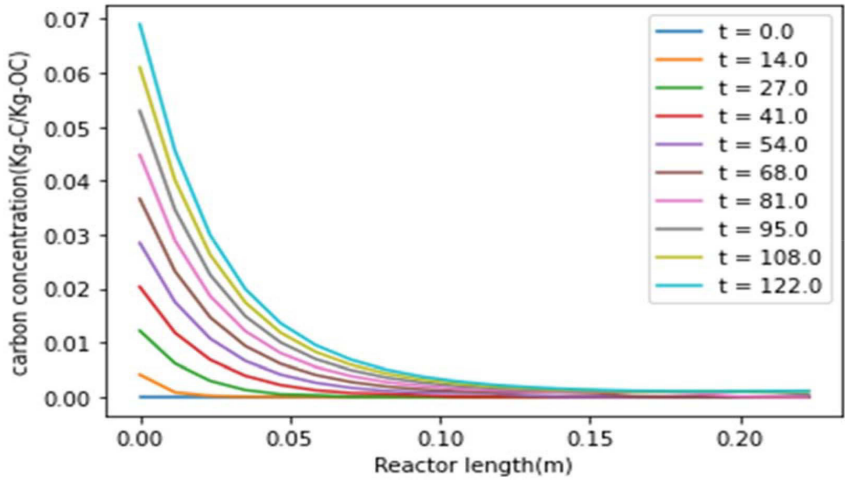


**Fig. 6** Spatial profiles of carbon at different reduction time instants.

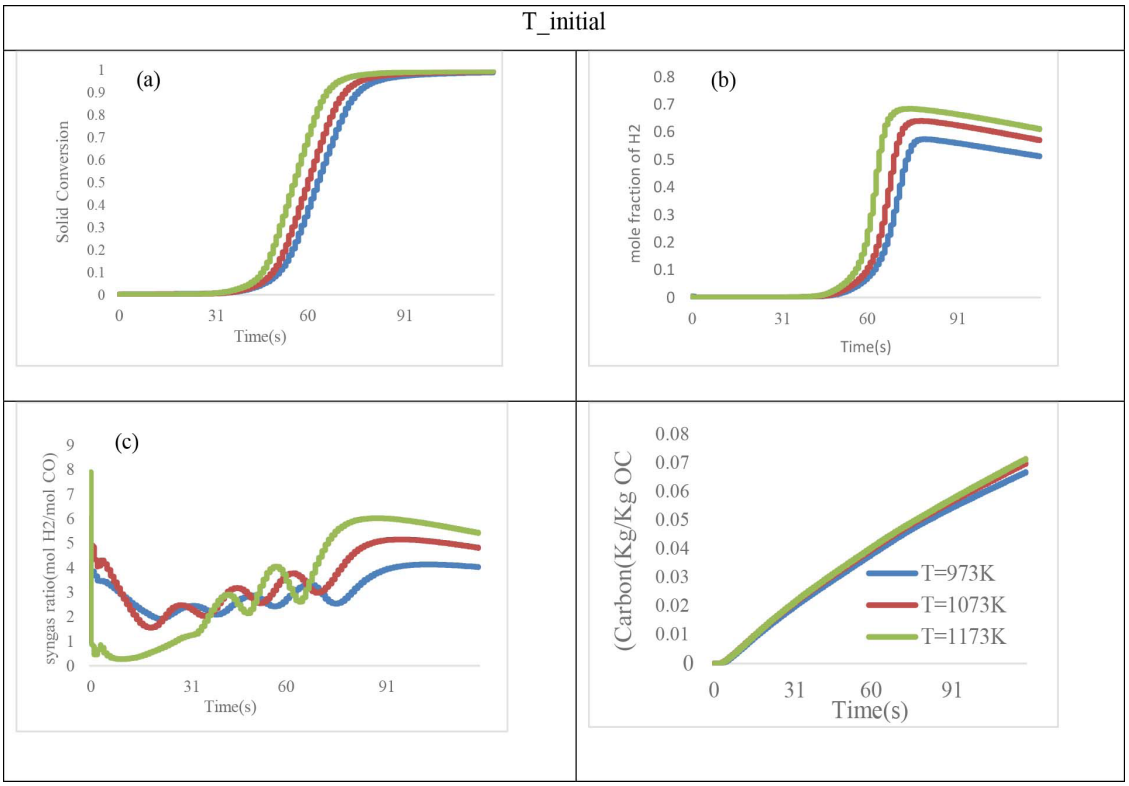


**Fig. 7** Effect of initial bed temperature on solid conversion of NiO (a), hydrogen production (b), Syngas ratio(c) and Carbon(d).

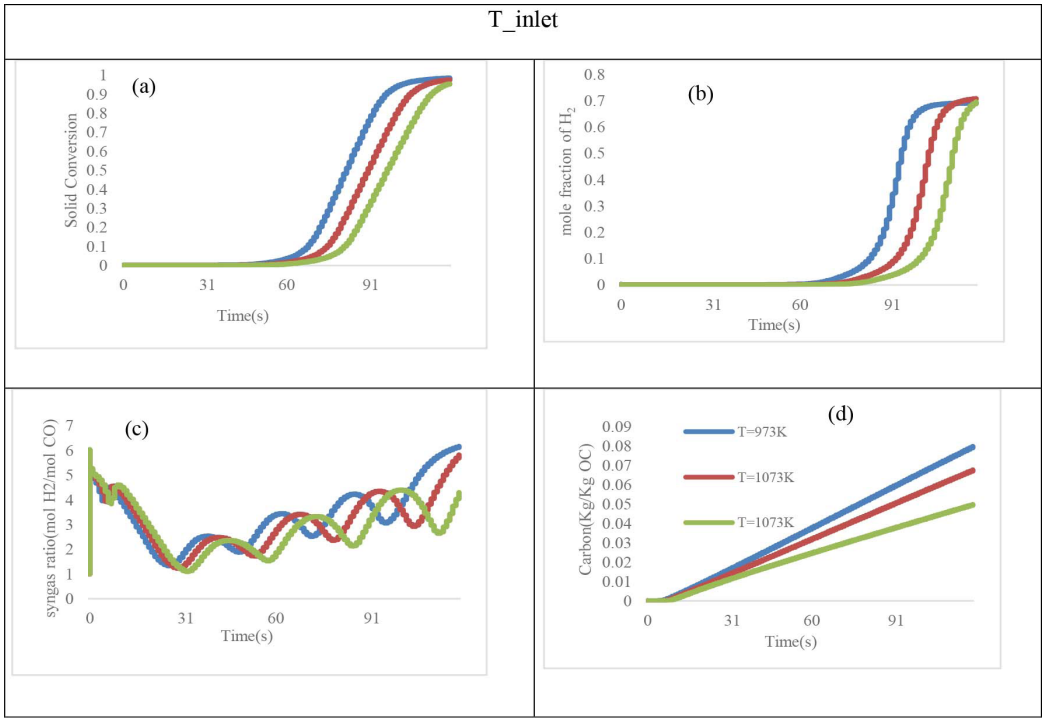


**Fig. 8** Effect of inlet bed temperature on solid conversion of NiO (a), hydrogen production (b), Syngas ratio (c) and Carbon (d).

## Temperature Profiles

Fig. 9 shows a 3D profile of temperature spatiotemporal in the reduction phase. While the endothermic reactions are starting, the temperature at the reactor outlet decreases to 1000 K after 75 seconds. As can be seen, the temperature decreases more at the reactor entrance. The temperature at the outlet of the air reactor During the exothermic reactions is shown in Fig. 10. Due to the heat released from the reactions, the temperature reaches 1073 K in 56 s.

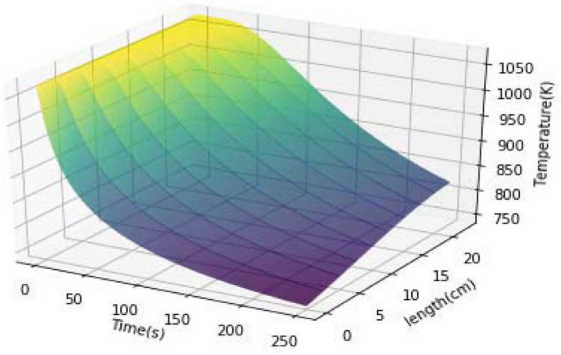


**Fig. 9** Temperature spatio-temporal pattern during the reduction phase.

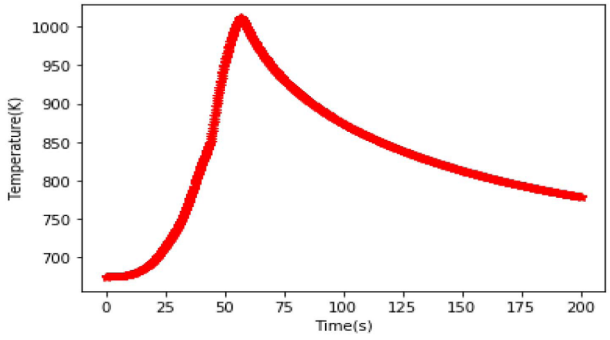


**Fig. 10** Temperature at the reactor exit during the oxidation phase.

## Comparison of NiO and Perovskite Oxygen Carriers

From an industrial point of view, the CLR reactor must be feasible. The fixed bed reactor could be fabricated and assembled in a series of reactors. In this process, the time between cycles is important for the design and feasibility. Here, two oxygen carriers of NiO and LSF731 are compared. Fig. 11 shows the solid conversion of the two oxygen carriers at different times during the reduction. At an inlet temperature of 723K in Fig.11 (a, b), while LSF731 is completely reduced (conversion is near one) during about 80000 s, only 120 s is enough for NiO to be converted entirely to Ni. This means that the reduction of NiO is 800 times faster than that of LSF731. In the case of perovskite, there is much time for the reduction in a cycle to be switched. In this situation, the perovskite is preferable for industrial applications, particularly in microscale geometries. According to Fig. 11 (d), with increasing temperature to 1173 K, the conversion is suddenly increased before 300 s, which is shown in the center plot in Fig.11 (d), while in Fig. 11(c), the NiO particles are converted gradually at the beginning.

## Effect of Changing Flowrate on the Reduction Time

One of the most influential factors in the reduction time is the flow rate of the reactants. In Fig. 12, as the flow rate increases, so do the reaction rates, decreasing the time required for the complete conversion. This is because more reactant reacts in the same amount of time.

## Syngas Ratio

The change in the hydrogen to carbon monoxide ratio, which differs for several applications, is shown in Fig. 13 during the process. It is seen that the maximum ratio reaches 5.5 at 85 s of the reduction near the reactor outlet. The average ratio of $H_2$/CO at the reactor outlet is 3.8. This ratio can be changed by injecting carbon dioxide or water vapor [7].

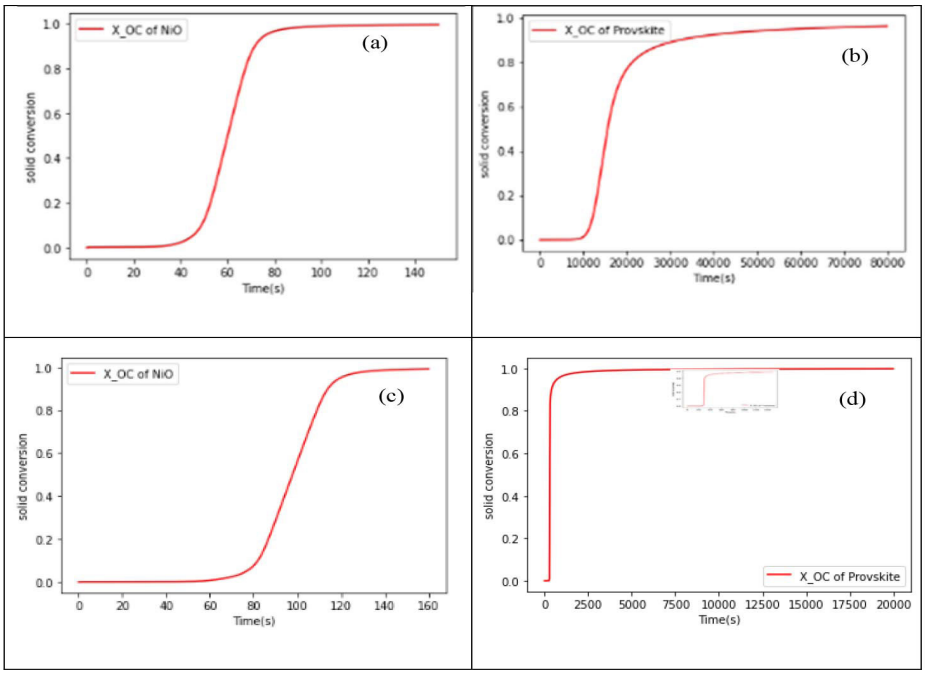


**Fig.11** Solid Conversion averaged at the outlet for two oxygen carriers of (a, c) NiO and (b, d) perovskite LSF731.

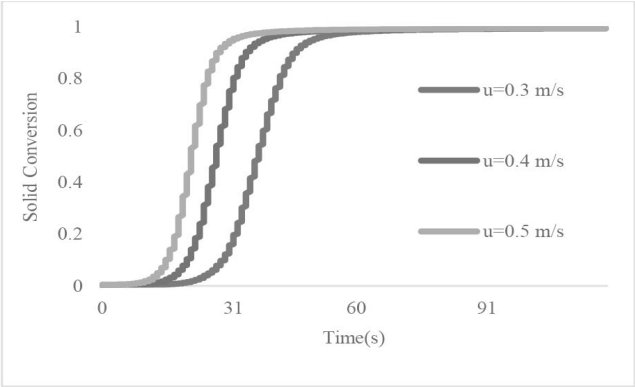


**Fig. 12** Solid Conversion at the reactor outlet for different flow rates.

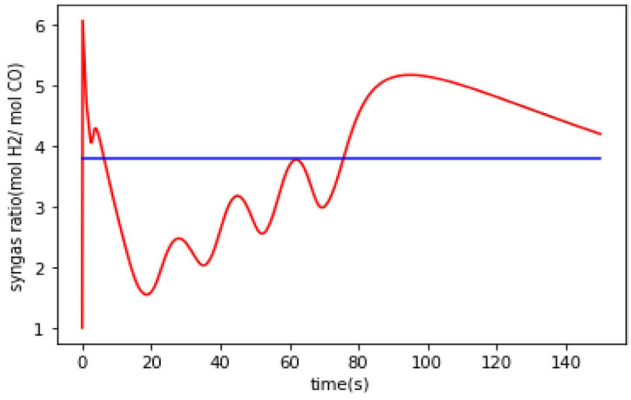


**Fig. 13** syngas ratio as a function of time.

Fig. 14 reports methane conversion, $X_{CH4}$ (a), and hydrogen yield at the outlet of the reforming section. In this figure, both methane conversion and hydrogen yield are illustrated in the reforming section. Methane has not reached the reactor outlet before 50 sec, so its concentration is zero, and according to Eq. (5), the maximum degree of methane conversion is one. After that, methane is completely consumed at 62s. From this time onwards, the outlet methane gradually increases while the conversion decreases, reaching 0.5 in 120s.

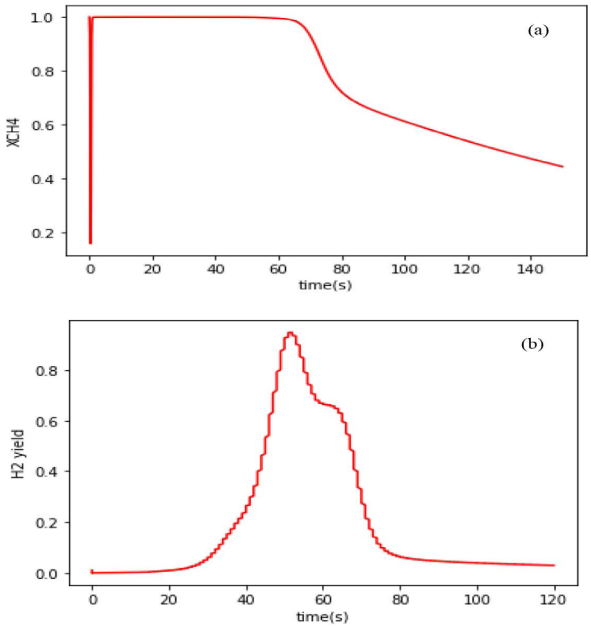


**Fig. 14** $CH_4$ conversion (a), $H_2$ yield (b) as a function of time during the reforming process.

The maximum value of $H_2$ yield in the reforming section at 62s is about 0.65 (mol $H_2$/mol $CH_4$) compared with those reported by Diglio et al. [6] under similar operating conditions.

$$X_{CH_4} = \frac{C_{CH_4,inlet} - C_{CH_4}}{C_{CH_4,inlet}} \quad (31)$$

## Cyclic Operation

Integrating oxidation and reduction processes in a geometry can lead to a reduction in energy consumption. This section will analyze the simulation results obtained from the cyclic operations. A cyclic operation consisting of a sequence of four stages of the reduction and oxidation with the period $T=t_{Red}+t_{Oxi}+2tpurge$ is considered, which is $t_{Red}$=120s, $t_{Oxi}$=63 sec, and $t_{purge}$=10s. Furthermore, Fig. 15 shows the molar fraction of the components in the reactor outlet during the cyclic operation of the system.

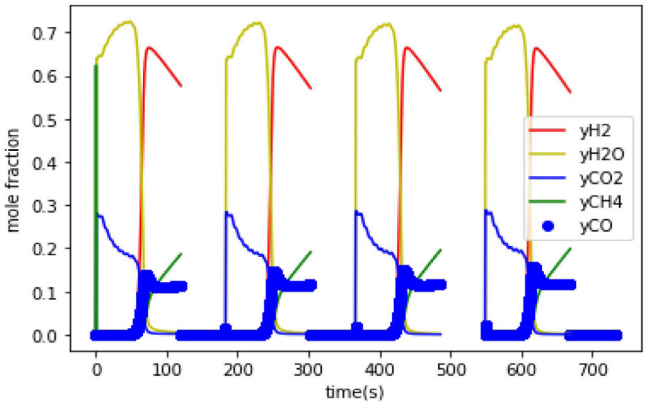


**Fig. 15** Outlet gas molar fractions during multiple OP/RP cycles.

The process starts with the reduction and a mixture of methane and water with a ratio of 3 to 1 injected into the system, after which nitrogen gas passes through the system as an inert gas within 10 seconds. Then, the oxidation stage starts, and the reactor is fed with air. After this step, the purge is performed again. The molar fraction of the components in the reactor output changes during the reduction time and has the same behavior as described in the previous section. After the completion of one cycle, the reduction phase starts again, and the operation continues. As can be seen, the regime conditions are established after three stages.

## CLR Operation of a Reactors' Network

According to the previous section, the duration of the reduction is 50% of the entire time period, so for the continuous production of hydrogen, more than one reactor is needed, which is arranged in a parallel structure. According to the ratio of the reduction time to the total duration and considering that no hydrogen is produced in the first 50 sec of the reduction time, the minimum number of reactors needed to have a continuous flow of hydrogen is four. In order to improve the continuity of the process, more number of reactors can be used.

Fig. 16 reports the time sequence of the operations of the CLR network: for each reactor, the big white zone represents the RP, the black zone the PP and the small white zone the OP. The following features emerge from an analysis of the figure: At the beginning of the operation, the oxygen carrier in the four reactors is completely oxidized. At t=0, methane and water are injected into the first reactor as the feed, so the reduction occurs until $t=t_{Red}$.

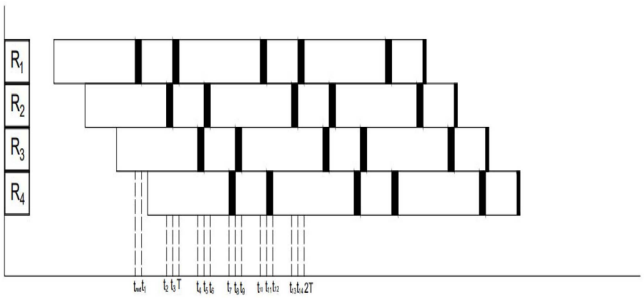


**Fig. 16** Time sequence of the operation of the reactor network in CLR.

After the 50 sec had passed in the first reactor, the second reactor was fed with methane and water and remained in the RP until $t=t_2=2t_{Red}$. At $t=t_{Red}$, the feed of the first reactor is changed to nitrogen for the removal operation, and this reactor will be in the PP until $t= t_1=t_{Red}+t_{purge}$. At $t=t_1$, the PP ends, and air enters the first reactor and continues until $t=t_3=t_{Red}+t_{purge}+t_{oxi}$.

At $t=t_2$, RP in the second reactor is completed. After 50 sec of the reduction time of the second reactor, the third reactor enters the reduction phase. At this time, the first reactor is located in the OP. The second reactor enters PP. At $t=t_3$, the oxidation in the first reactor is completed, and PP starts and continues until T. At T, the new cycle of the first reactor starts with RP, and the second reactor is in the oxide phase. At $t=t_3$, PP ends in the second reactor, and OP begins and continues until $t=t_5$. At this stage, the first and third reactors are located in the RP. At $t=t_5$, PP starts in the second reactor and continues until $t=t_6$. The first reactor is in RP, and the third reactor starts the OP and continues until $t=t_8$. In the same way, this process is performed for three cycles in each reactor, and finally, we reach a continuous production of hydrogen. The outlet gas molar fractions at the exit of reforming were reported in Fig. 17: clearly, a continuous production of hydrogen ( is about 0.67) can be achieved at the periodic regime conditions.

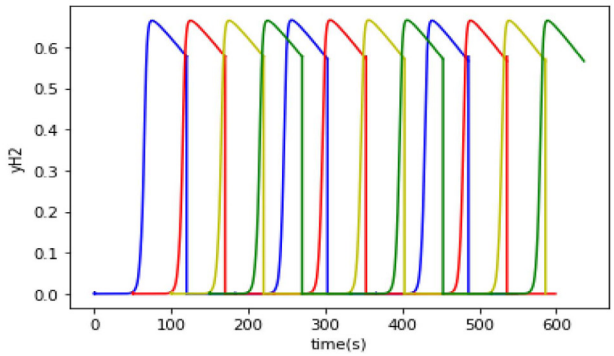


**Fig. 17** Hydrogen molar fraction at the outlet of reforming as a function of time (blue: reactor 1, red: reactor 2, yellow: reactor 3, green: reactor 4).

## Conclusion

In this study, a syngas production process in a sequential fixed-bed reactor network was proposed. The developed CLR arrangement consists of the four packed operated continuously to produce a mixture of $H_2$ and CO. According to the ratio of the reduction time to the whole time of the process and considering that no hydrogen is produced in the first 50s of the reduction time, the minimum number of reactors needed to have a continuous flow of hydrogen is four. The numerical results revealed a strong influence of the reduction time, initial and inlet temperature on the process feasibility.

The mathematical model was validated through the experimental results available in the literature. H2-rich gas stream with an average $Y_{H_2}$ of 0.67 was evaluated. The numerical results revealed that while a complete reduction of $La_{0.7}Sr_{0.3}FeO_3$ was obtained at about 80000 s, only 120 s was enough for NiO particles to be reduced entirely. In the case of perovskite, there is much time for the reduction in a cycle to be switched. The high delay time for switching the feed stream (fuel/purge/oxidant/) is helpful for handling,

However, there are some applications that the reduction step must be kept on. In this situation, the perovskite is preferable for some industrial applications, particularly in microscale geometries. Several important parameters such as product composition and inlet and initial temperature were analyzed. $H_2$/CO ratio, $H_2$ yield and methane conversion were also investigated. This model does not mention the coke burning process in the oxidation phase, so it can be considered as the next stage of model modification.

**Nomenclature**

$a_0$: The initial specific surface area of the oxygen carrier ($m^2$ $kg^{-1}$)
$K_{si}$: the reaction rate constant, m/s
$K_{R_1}$: the reaction rate constant of SR (mol $kg^{-1}{}_{Ni}$ $s^{-1}$ $bar^{-0.25}$)
$K_{R_2}$: the reaction rate constant of DR (mol kg−1Ni s−1 $bar^{-2}$)
$K_{R_3}$: the reaction rate constant of methane decomposition (mol $kg^{-1}$Ni $s^{-1}$)
$K_{R_5}$:the reaction rate constant of WGS (mol $kg^{-1}{}_{Ni}$ $s^{-1}$ $bar^{-1}$)
$K_{R_6}$: the reaction rate constant of carbon gasification by $CO_2$ (mol $kg^{-1}$Ni $s^{-1}$)
$K_{R_7}$: the reaction rate constant of carbon gasification by $H_2O$ (mol $kg^{-1}$Ni $s^{-1}$)
$K_{P,R_1}$: equilibrium constant of SR (bar2)
$K_{P,R_3}$: the equilibrium constant of methane decomposition (bar)
$K_{P,R_5}$: equilibrium constant of WGS (mol $kg^{-1}{}_{Ni}$ $s^{-1}$ bar)
$K_{P,R_6}$: equilibrium constant of carbon gasification by $CO_2$ (–)
$K_{P,R_7}$: equilibrium constant of carbon gasification by $H_2O$ (bar)
$K_{CO,R_1}$: Radsorption coefficient of CO (steam reforming) ($bar^{-1}$)
$K_{H_2,R_1}$: adsorption coefficient of $H_2$ (steam reforming) ($bar^{-0.5}$)
$K_{H_2,R_1}$: adsorption coefficient of $H_2O$ (steam reforming) (–)
$K_{CO_2,R_2}$: adsorption coefficient of $CO_2$(dry reforming) ($bar^{-1}$)
$K_{CH_4,R_3}$: adsorption coefficient of $CH_4$ (methane decomposition) ($bar^{-1}$)
$K_{H_2O,R_3}$: adsorption coefficient of $H_2$ (methane decomposition) ($bar^{1.5}$)
$K_{H_2O,R_7}$ adsorption coefficient of $H_2$ (carbon gasification by $H_2O$) ($bar^{1.5}$)
$K_{CH_4,R_7}$: adsorption coefficient of $CH_4$ (carbon gasification by $H_2O$) ($bar^{-1}$)
$K_{H_2O,R_7}$: adsorption coefficient of $H_2O$ (carbon gasification by $H_2O$) (–)
$K_{CO,R_6}$: adsorption coefficient of CO (carbon gasification by $CO_2$) ($bar^{-1}$)
$K_{CO_2,R_6}$: adsorption coefficient of $CO_2$ (carbon gasification by $CO_2$) (bar)
$r_{R_i}$: Rate of reaction, kmol $Kg^{-1}{}_{Ni}S_{-1}$
$u_g$: velocity, m/s
$C_{p,g}$: heat capacity of the gas stream (J $mol^{-1}$ $K^{-1}$)
$C_{T,g}$: Total concentration of the gas stream ($molL^{-1}$)
$D_i$: axial dispersion coefficient of species i ($m^2$ $s^{-1}$)
$M_i$: molecular weight of *i* species, (kg $mol^{-1}$)
Le: Lewis number (J $m^{-3}$ K)
$E_{a,ij}$: activation energy of adsorption coefficient of specie i in reaction j (J $mol^{-1}$)
$E_{a,j}$: activation energy of reaction rate of reaction j (J $mol^{-1}$)
$E_{a,si}$ activation energy of non-catalytic gas–solid reactions (J $mol^{-1}$)
$E_{ap,j}$: activation energy of equilibrium constant (J $mol^{-1}$)
$E_2$: activation energy of equilibrium constant (J $mol^{-1}$)
$E_1$: activation energy of equilibrium constant (J $mol^{-1}$ $K^{-1}$)
$K_{i,R_j,0}$: pre-exponential factor of adsorption coefficient of specie *i* in reaction *j*
$K_{P,R_j,0}$: pre-exponential factor of equilibrium constant cycle index
$K_{R_j,0}$: pre-exponential factor of reaction rate constant
T: temperature (K)
$R_m$: gas universal constant, J/mol.K
$C^0_{Nio}$: initial NiO concentration($kg^{-1}{}_{OC}$)
$C^0_{Ni}$: initial concentration of Ni ($kg^{-1}{}_{OC}$)
$D_{ax,i}$: axial dispersion coefficient of species i ($m^2$ $s^{-1}$)
$r_i$: Reaction rate of gas component i, (kmol $kg^{-1}{}_{OC}S^{-1}$)
L: bed length (m)
$d_t$: reactor internal diameter (m)
$d_p$: particle diameter (m)
$r_j$: reaction rate of solid component j, (kmol $kg^{-1}{}_{OC}S^{-1}$)
X: Solid conversion

**Greek Letters**

$\rho_{oC}$: packed-bed density (kgOC $m^{-3}$)
$\Delta Hj$: reaction enthalpy of reaction j (J $mol^{-1}$)
$\varepsilon_g$: bed porosity (–)
$\lambda_{ax}$: axial heat dispersion (W $m^{-1}$ $K^{-1}$)
$\lambda_{eff}$:effective heat dispersion (W $m^{-1}$ $K^{-1}$)

**Abbreviations**

CLR: chemical looping reforming
OP: oxidation phase
RP: reduction phase
PP: purge phase
SR: steam reforming
WGS: water gas shift

**References**

1. Aasberg-Petersen K, Bak Hansen JH, Christensen TS, Dybkjaer I, Christensen PS, Stub Nielsen C, et al. Technologies for large-scale gas conversion. Appl Catal A Gen. 2001;221(1–2):379–87.
2. Ott, J., Gronemann, V., Pontzen, F., Fiedler, E., Grossman, G., Burkhard Kersebohm, K., Weiss, G. & Witte, C. (2012). Methanol-an industrial review by lurgi gmbh, air liquide gmbH and BASF AG. Ullmann's Encyclopedia of Industrial Chemistry.
3. Ebrahimi H, Rahmani M. Modeling chemical looping syngas production in a microreactor using perovskite oxygen carriers. Int J Hydrogen Energy [Internet]. 2018;43(10):5231–48. Available from: doi.org/10.1016/j.ijhydene.2018.01.108.
4. Spallina V, Marinello B, Gallucci F, Romano MC, Van Sint Annaland M. Chemical looping reforming in packed-bed reactors: Modelling, experimental validation and large-scale reactor design. Fuel Process Technol [Internet]. 2017;156:156–70. Available from: dx.doi.org/10.1016/j.fuproc.2016.10.014.
5. Diglio G, Bareschino P, Solimene R, Mancusi E, Pepe F, Salatino P. Numerical simulation of hydrogen production by chemical looping reforming in a dual fluidized bed reactor. Powder Technol [Internet]. 2017;316:614–27. Available from: http://dx.doi.org/10.1016/j.

powtec.2016.12.051.
6. Diglio G, Bareschino P, Mancusi E, Pepe F. Novel quasi-autothermal hydrogen production process in a fixed-bed using a chemical looping approach: A numerical study. Int J Hydrogen Energy [Internet]. 2017;42(22):15010–23. Available from: dx.doi.org/10.1016/j.ijhydene.2017.05.017
7. Ebrahimi H, Rahmani M. A novel intensified microreactor for syngas production by coupling reduction-oxidation reactions in chemical looping reforming process. J Clean Prod. 2017;167:376–94.
8. Iliuta I., Tahoces R., Patience G.S., Rifflart S., Luck F., Chemical-Looping Combustion Process: Kinetics and Mathematical Modeling. AIChE J. 2012;59(4):215–28.
9. Diglio G, Bareschino P, Mancusi E, Pepe F. Simulation of hydrogen production through chemical looping reforming process in a packed-bed reactor. Chem Eng Res Des [Internet]. 2016;105:137–51. Available from: dx.doi.org/10.1016/j.cherd.2015.11.013
10. Ebrahimi H, Rahmani M. Hydrogen production in membrane microreactor using chemical looping combustion: A dynamic simulation study. Int J Hydrogen Energy [Internet]. 2017;42(1):265–78. Available from: dx.doi.org/10.1016/j.ijhydene.2016.11.174
11. Ebrahimi H, Rahmani M. A novel intensified microreactor for syngas production by coupling reduction-oxidation reactions in chemical looping reforming process. J Clean Prod [Internet]. 2017;167:376–94. Available from: dx.doi.org/10.1016/j.jclepro.2017.08.143
12. Cox KR, Chapman WG. The Properties of Gases and Liquids, 5th Edition By Bruce E. Poling (University of Toledo), John M. Prausnitz (University of California at Berkeley), and John P. O'Connell (University of Virginia). McGraw-Hill: New York. 2001. 768 pp. $115.00. ISBN 0-07-0. Vol. 123, Journal of the American Chemical Society. 2001. 6745–6745 p.
13. Fogler HS. Scilab code for elements of chemical reaction engineering. Education. 2010. 104 p.
14. Han L, Zhou Z, Bollas GM. Heterogeneous modeling of chemical-looping combustion. Part 1: Reactor model. Chem Eng Sci. 2013;104:233–49.
15. Dueso C, Ortiz M, Abad A, García-Labiano F, De Diego LF, Gayán P, et al. Reduction and oxidation kinetics of nickel-based oxygen-carriers for chemical-looping combustion and chemical-looping reforming. Chem Eng J [Internet]. 2012;188(x):142–54. Available from: dx.doi.org/10.1016/j.cej.2012.01.124.
16. Chiron, F. X., Patience, G. S., & Rifflart, S. (2011). Hydrogen production through chemical looping using $NiO/NiAl_2O4$ as oxygen carrier. Chemical Engineering Science, 66(24), 6324-6330. doi.org/10.1016/j.ces.2011.03.060.